Human Molecular Genetics, 2008, Vol. 17, No. 14 **2132–2143**
doi:10.1093/hmg/ddn112
Advance Access published on April 22, 2008

AAV-mediated intramuscular delivery of myotubularin corrects the myotubular myopathy phenotype in targeted murine muscle and suggests a function in plasma membrane homeostasis

Anna Buj-Bello[1,*], Françoise Fougerousse[4], Yannick Schwab[2], Nadia Messaddeq[2], Danièle Spehner[3], Christopher R. Pierson[5,†], Muriel Durand[4], Christine Kretz[1], Olivier Danos[4,‡], Anne-Marie Douar[4], Alan H. Beggs[5], Patrick Schultz[3], Marie Montus[4], Patrice Denèfle[4] and Jean-Louis Mandel[1]

[1]Department of Neurobiology and Genetics, [2]Imaging Center – Electron Microscopy and [3]Department of Structural Biology and Genomics, Institut de Génétique et de Biologie, Moléculaire et Cellulaire (IGBMC), INSERM U596, CNRS UMR 7104, Université Louis Pasteur de Strasbourg, Collège de France, 67404 Illkirch, France, [4]Généthon, R&D Department, 1 rue de l'Internationale, 91000 Evry and [5]Children's Hospital, Harvard Medical School, Boston, USA

Received December 10, 2007; Revised and Accepted April 8, 2008

Myotubular myopathy (XLMTM, OMIM 310400) is a severe congenital muscular disease due to mutations in the myotubularin gene (*MTM1*) and characterized by the presence of small myofibers with frequent occurrence of central nuclei. Myotubularin is a ubiquitously expressed phosphoinositide phosphatase with a muscle-specific role in man and mouse that is poorly understood. No specific treatment exists to date for patients with myotubular myopathy. We have constructed an adeno-associated virus (AAV) vector expressing myotubularin in order to test its therapeutic potential in a XLMTM mouse model. We show that a single intramuscular injection of this vector in symptomatic *Mtm1*-deficient mice ameliorates the pathological phenotype in the targeted muscle. Myotubularin replacement in mice largely corrects nuclei and mitochondria positioning in myofibers and leads to a strong increase in muscle volume and recovery of the contractile force. In addition, we used this AAV vector to overexpress myotubularin in wild-type skeletal muscle and get insight into its localization and function. We show that a substantial proportion of myotubularin associates with the sarcolemma and I band, including triads. Myotubularin overexpression in muscle induces the accumulation of packed membrane saccules and presence of vacuoles that contain markers of sarcolemma and T-tubules, suggesting that myotubularin is involved in plasma membrane homeostasis of myofibers. This study provides a proof-of-principle that local delivery of an AAV vector expressing myotubularin can improve the motor capacities of XLMTM muscle and represents a novel approach to study myotubularin function in skeletal muscle.

INTRODUCTION

Myotubular myopathy (XLMTM, OMIM 310400) is the X-linked and most severe form of a group of muscular disorders, named centronuclear myopathies (CNM), characterized by the presence of hypotrophic myofibers with central nuclei in skeletal muscle (1). Myotubular myopathy, which

*To whom correspondence should be addressed at: Department of Neurobiology and Genetics, Institut de Génétique et de Biologie, Moléculaire et Cellulaire (IGBMC), 1, rue Laurent Fries, BP 10142, 67404 Illkirch, France. Tel: +33 388653244; Fax: +33 388653246; Email: mtm@igbmc.u-strasbg.fr
†Present address: Research Institute at Nationwide Children's Hospital, Columbus, USA.
‡Present address: INSERM U781, Hôpital Necker-Enfants Malades, Paris, France.

affects one newborn male in 50 000 is caused by mutations in the ubiquitously expressed *MTM1* gene that codes for a phosphoinositide phosphatase named myotubularin (2,3). Missense mutations in DNM2 (dynamin 2) are found in most patients in the autosomal dominant form (4,5), and recently, mutations in amphiphysin 2/Bin1, a dynamin 2 interactor, have been found in some patients with autosomal recessive CNM (6). XLMTM patients are born with generalized hypotonia and muscle weakness leading to respiratory difficulties, and most of them either die during early postnatal life or survive with intensive medical care (7,8). Skeletal muscle from XLMTM patients contains hypotrophic fibers with central nuclei surrounded by a halo devoid of myofibrils where mitochondria and glycogen accumulate (9,10). Fiber size, but not the proportion of myofibers with central nuclei, shows a correlation with clinical outcome (11). Mice deficient for *Mtm1* have been generated and presented a clinical and pathological phenotype similar to the human condition (12). These mice are born with normally differentiated muscle, but develop a progressive CNM starting at around 3–4 weeks of age, with amyotrophy and structural myofiber disorganization, leading to death at ~6–12 weeks. As muscle differentiation and maturation appear normal in these mice, we have proposed that defects in maintenance of muscle cell architecture are responsible for the internalization of nuclei and other organelles. The same phenotype is observed when the *Mtm1* gene is inactivated only in skeletal muscle, indicating that myotubularin exerts a muscle autonomous function (12).

MTM1 belongs to a large disease-associated gene family with 14 members in humans, including *MTMR2* and *MTMR13*, which are mutated in demyelinating Charcot-Marie-Tooth type 4B1 and 4B2 neuropathies, respectively (13–16). Myotubularins are subdivided into active and inactive phosphatases (16). Active family members dephosphorylate specific phosphoinositides, PtdIns3*P* and PtdIns(3,5)P_2, which are lipid second messengers mainly associated with endosomes, and appear involved in the regulation of endocytic pathways (17). Most myotubularins are cytoplasmic proteins that also associate with peripheral and/or internal membranes, as investigated in overexpression systems (18–22). In particular, the MTM1 protein appears cytoplasmic in various cell lines and has been found associated with endosomes (20,23). Its overexpression induces the formation of filopodia-like projections and affects protein trafficking from late endosome to lysosome (20,24). No data have been reported up to date on the subcellular localization and specific function of myotubularin in muscle fibers.

Recombinant adeno-associated viruses (rAAV) represent a powerful tool to express transgenes *in vivo*, and several serotypes transduce with high efficiency skeletal muscle (25). In order to evaluate the feasibility for viral-mediated *Mtm1* gene transfer as a therapeutic approach, we have injected an rAAV2/1 vector containing the *Mtm1* cDNA into skeletal muscle of XLMTM mice. Our results demonstrate that myotubularin replacement in a mouse model of the disease is sufficient to correct the pathology and strength of affected muscles and thus opens novel perspectives for therapy in patients with myotubular myopathy. Furthermore, AAV-mediated expression of myotubularin in skeletal muscle can also be used for functional analysis. Its overexpression in wild-type (WT) muscle generates a striking proliferation of membrane structures that contain myotubularin and the presence of vacuoles that are labeled by markers of sarcolemma and T-tubules. Vacuoles present in *Mtm1*-deficient muscle appear also derived from sarcolemma and T-tubules. These results suggest that myotubularin regulates plasma membrane homeostasis and/or remodeling in skeletal muscle.

RESULTS

Skeletal muscle pathology of *Mtm1*-deficient mice before AAV-mediated gene transfer

Constitutive and muscle-specific *Mtm1*-deficient mice develop a progressive and generalized myopathy starting at 3–4 weeks of age and leading to early death (12). We have assessed the efficacy of viral-mediated *Mtm1* transduction in the muscle-specific mutant line (Mtm1/HSA = mKO) to avoid an immunological reaction against the transgene. The tibialis anterior (TA) muscle of 4 week-old muscle-specific knockout (mKO) mice was selected for rAAV vector injection, a widely used muscle for gene therapy experiments, because weakness was already present in hindlimbs at this age (animals were in clinical phase II, see 12). At 4 weeks of age, the weight of the TA muscle is lower by ~40% in muscle-specific mutant (mKO) compared with WT mice (Fig. 1A) and the mean area of TA muscle fibers is significantly smaller ($428 \pm 170\ \mu m^2$ in mKO versus $639 \pm 217\ \mu m^2$ in WT animals, $P < 0.001$, Fig. 1B), with the presence of many very small myofibers (23% of them being $<230\ \mu m^2$) that are not present in WT muscle at this age (Fig. 1B and C). Within muscle fibers, mitochondria appears already mislocalized at this stage of the disease, as assessed by oxidative staining, whereas most nuclei are still at their normal position beneath the sarcolemma (Fig. 1C).

Intramuscular injection of a rAAV2/1-Mtm1 vector ameliorates the histological phenotype of myotubularin-deficient muscle

To explore the efficacy of *Mtm1* cDNA replacement in blocking the progression of XLMTM muscle pathology, we injected 9×10^{10} vg of rAAV2/1-CMV-Mtm1 into the TA of 4 week-old Mtm1/HSA male mice. The contralateral muscle was injected with phosphate-buffered saline (PBS) as an internal control. Since the myopathy progresses rapidly and mice die early during postnatal life (at mean age of 56 days), the effect of AAV-mediated myotubularin expression was analyzed 4 weeks after injection. Immunofluorescence analysis of AAV-transduced mKO muscle cross-sections using novel polyclonal antibodies (discussed later) demonstrated that overexpressed myotubularin is present in most myofibers (Fig. 2A) and located throughout the cytoplasm with a clear reinforcement in the sarcolemmal region. Figure 2B shows that myotubularin re-expression in *Mtm1*-deficient muscle leads to a doubling in muscle mass (26.5 ± 3.1 mg in transduced compared with 12.3 ± 1.7 mg in mKO TA) that correlates with an increase in the volume of myofibers. Indeed, the mean area of AAV-treated mutant muscle fibers is three times larger than that of mKO mice

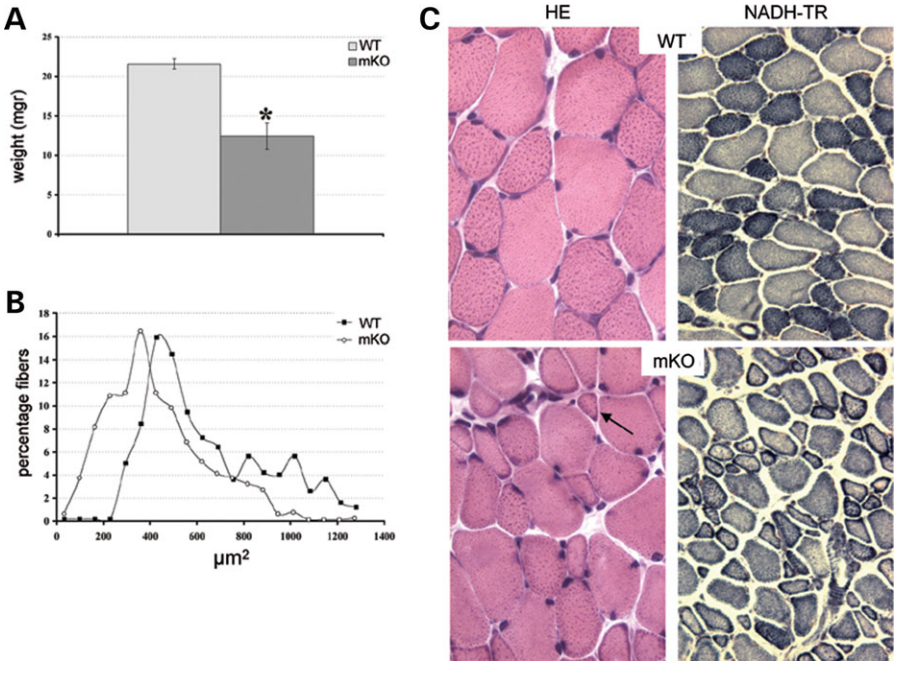

Figure 1. Pathology of tibialis anterior (TA) muscle of 4 week-old *Mtm1* mutant mice. (**A**) Weight of wild-type (WT) and Mtm1/HSA [mKO (muscle-specific knockout)] TA muscles ($n = 4$ and 8 muscles for WT and mKO, respectively). Note the important reduction of muscle mass in mutant mice ($^*P < 0.001$). (**B**) Area of TA myofibers. The curve represents the percentage of muscle fibers per area group (myofiber areas were divided into 20 groups, $n = 496$ and 771 for WT and mKO fibers, respectively, $P < 0.001$). The curve is shifted to the left in mKO animals indicating a general decrease of myofiber areas. (**C**) Hematoxylin and eosin (left panels, HE, magnification $\times 400$) and nicotimanide adenine dinucleotide tetrazolium reductase (NADH-TR) (right panels, magnification $\times 200$) staining of TA cross-sections from WT (top) and mKO (bottom) mice at 4 weeks of age. Note the presence of very small myofibers (arrow) and nuclei beneath the sarcolemma. Mitochondrial oxidative staining is often distributed as a ring at the periphery of the muscle fibers.

($970{,}76 \pm 338{,}24\ \mu m^2$ in mKO-AAV versus $314.05 \pm 129.34\ \mu m^2$ in mKO-PBS), and corresponds to ~50% of the mean area of WT muscle fibers ($1784.91 \pm 644.3\ \mu m^2$, Fig. 2C). Analysis of the distribution of myofiber areas shows a clear shift of the curve to the right, indicating an overall increase of the volume of treated muscle fibers (Fig. 2D). The percentage of myofibers with an area $<533\ \mu m^2$ shifts from 93% in the mKO population to only 18% after AAV treatment. In addition to fiber hypotrophy, centronucleation represents another hallmark of XLMTM pathology. We thus counted the number of fibers with internal nuclei in treated versus untreated TA muscle and observed a strong reduction in the percentage of fibers with internalized nuclei 4 weeks after viral injection (10.3% in treated compared with 26.5% in untreated mutant muscle, Fig. 3A). Finally, murine myotubularin-deficient muscle fibers are also characterized by a progressive disorganization of the distribution of organelles. Thus, we evaluated the location of mitochondria and endoplasmic reticulum by nicotimanide adenine dinucleotide tetrazolium reductase (NADH-TR) staining in mKO myofibers after rAAV2/1-CMV-Mtm1 transfer. Figure 3B shows that the morphology of mutant muscle fibers is restored by AAV treatment, as well as the internal architecture, since the distribution of the oxidative enzyme activity is similar to WT muscle. Similar results were obtained when sections were stained for succinate dehydrogenase activity, which reflects mitochondrial function (data not shown). Vacuoles that are observed in a small proportion of *Mtm1*-deficient myofibers at 8 weeks of age (but not at 4 weeks) (12) are decreased in number in transduced fibers (data not shown). Occasional small foci of inflammatory infiltrates were observed in AAV-transduced mKO muscles, often nearby myofibers expressing high levels of myotubularin (Fig. 3C). Altogether, our results demonstrate that a single intramuscular injection of a rAAV vector carrying a *Mtm1* cDNA is sufficient to ameliorate the pathology of an already affected XLMTM muscle.

Myotubularin replacement restores the contractile force of *Mtm1* mutant muscle

We tested whether AAV-mediated myotubularin replacement could be beneficial at the functional level because muscle weakness is the constant and life threatening sign of the disease. Briefly, 2.5 and 9×10^{10} vg of rAAV2/1-CMV-Mtm1 were injected into the right extensor digitorum longus (EDL) and TA muscles of 4 week-old mKO mice, respectively. Four weeks later, mice were anesthetized and muscles excised for *in vitro* measurement of the force. Like TA, the EDL showed a clear increase in muscle mass (5.7 ± 0.5 mg in mKO-AAV compared with 3.6 ± 0.1 mg in mKO-PBS EDL muscle, $n = 6$ for each group, $P < 0.0006$), indicating that AAV transduction and myotubularin expression were also efficient in this muscle, see Figure 4A. We measured the specific isometric force of untreated EDL and TA muscles of 8 week-old myotubularin-deficient mice and found that strength was lower by ~80% in both muscles compared with WT (Fig. 4B). No difference in the resistance of mKO muscles to mechanical stretch was

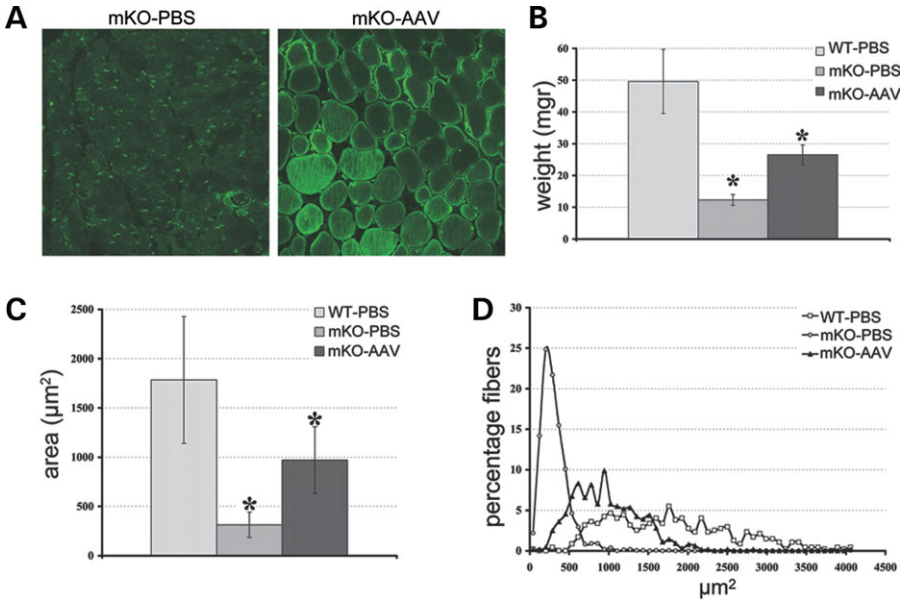

Figure 2. Myotubularin replacement leads to increased muscle volume. (**A**) Expression of myotubularin in muscle-specific knockout (mKO) muscle after rAAV2/1 transduction. phosphate-buffered saline (PBS) and adeno-associated virus (AAV)-treated mutant tibialis anterior (TA) cross-sections (mKO-PBS and mKO-AAV) were immuno-labeled with a rabbit polyclonal antibody against myotubularin. The antibody labels aspecifically nuclei in mutant muscle, whereas it detects myotubularin throughout the fiber with reinforcement in the sarcolemmal region 4 weeks after rAAV2/1-CMV-Mtm1 vector transfer (magnification $\times 400$). (**B**) Weight of mutant TA muscle after myotubularin re-expression. The weight of isolated TA was measured 4 weeks after viral transduction (mKO-AAV) and compared with PBS-injected wild-type (WT) and mKO muscles ($n = 6$ for WT-PBS and mKO-AAV, $n = 7$ for mKO-PBS). The weight is lower by about four times in mutant animals (mKO-PBS, $^*P = 2 \times 10^{-6}$), but significantly increased after rAAV (recombinant AAV) transfer ($^*P = 2 \times 10^{-5}$). (**C**) Evaluation of mean myofiber area 4 weeks after intramuscular injection of rAAV2/1-CMV-Mtm1 vector. The size of *Mtm1*-deficient TA muscle fibers is smaller than WT animals ($n = 473$ from five mice and $n = 1555$ from four mice for WT-PBS and mKO-PBS, respectively, $^*P < 0.001$). Viral transduction leads to a strong increase in myofiber area ($n = 636$ from four mice for mKO-AAV, $^*P < 0{,}001$). (**D**) Distribution of muscle fibers from TA according to their size. The areas were subdivided into 20 subgroups ranging from the smallest to the biggest area, the interval between each subgroup corresponds to 82 μm^2. The curve represents the percentage of fibers that belongs to each of the subgroups according to genotype and treatment. Note the strong reduction of very small fibers in mKO-AAV muscle.

observed, as tetanic force values remained similar after a series of five eccentric contractions (data not shown). Importantly, viral-mediated myotubularin expression led to the correction of EDL and TA muscle-specific forces in mutant mice, reaching a level similar to WT animals (Fig. 4B). The strength of EDL muscles 4 weeks after AAV injection represents $\sim$75% that of normal muscles and the tension of treated TA muscles is not significantly different than of WT muscles. This functional recovery could even be visualized at the clinical level, as mice were able to climb on objects more efficiently than untreated mice and could grasp on objects with their AAV-treated hindlimbs (Supplementary Material, Video).

Localization of myotubularin in skeletal muscle

The specific function of myotubularin and its subcellular localization in skeletal muscle are presently unknown. Previous attempts to localize the endogenous protein by immunohistological methods have failed (unpublished data). We raised a novel polyclonal antibody against the C-terminal part of mouse myotubularin and show that it detects the endogenous protein by direct western blotting (Fig. 5A), while all previously generated monoclonal and polyclonal antibodies required an additional immunoprecipitation step (20). This antibody does not cross-react with either mouse MTMR1 or MTMR2 (the closest paralogues of MTM1), as assessed by transfection of expression plasmids in COS cells (data not shown). Myotubularin is ubiquitously expressed in mouse tissues, being more abundant in striated muscles than in sciatic nerve and brain, and increases during the first postnatal week in skeletal muscle (Supplementary Material, Fig. S1). The sensitivity of this novel antibody in skeletal muscle is rather low by immunohistochemistry but was sufficient to detect endogenous myotubularin on semithin sections (Fig. 5B). Specific myotubularin labeling was found in a region of the I-band and appeared as two distinct bands flanking markers of the Z-line (α-actinin). These bands colocalize with markers of the triad (ryanodine receptor and triadin). A third band in the region of the M-line, is detectable in *Mtm1* KO mice and represents a cross-reacting, but unrelated protein. We failed, however, to detect endogenous myotubularin at the ultrastructural level. In order to increase sensitivity, we further analyzed myotubularin localization overexpressed in the TA of WT mice, 4 weeks after injection of 9×10^{10} vg of the rAAV2/1-CMV-Mtm1 vector. Specific staining for myotubularin was found at the sarcolemma and in a region of the I-band, where staining also appears predominantly around the Z-line as a double row (Fig. 5B). To further investigate the precise location within the I-band, we performed immunoelectron microscopy on muscle sections and found that myotubularin associates with the triad, a specialized

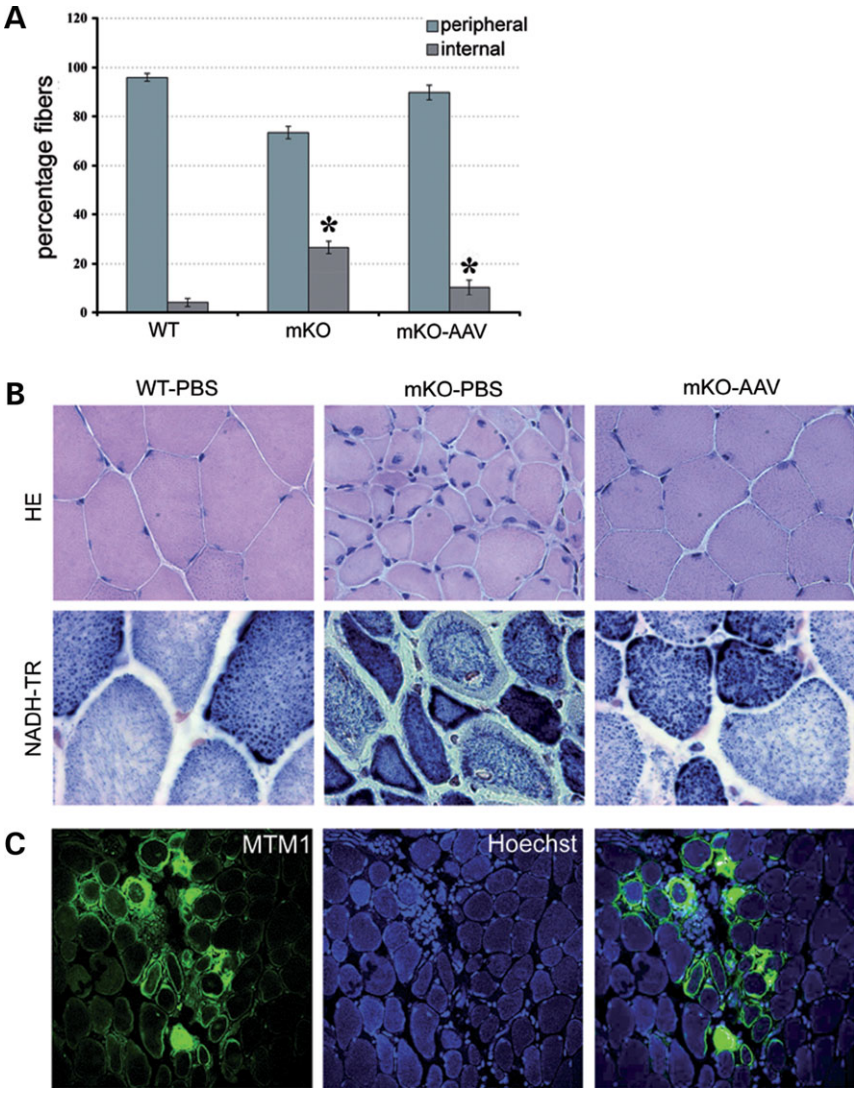

Figure 3. Correction of XLMTM (X-linked myotubular myopathy) pathology by viral-mediated myotubularin treatment. (**A**) Percentage of muscle fibers with internalized nuclei after adeno-associated virus (AAV)-mediated myotubularin expression. Myonuclei were considered as internalized if detached from the sarcolemma. The number of fibers with internal nuclei is increased in mutant tibialis anterior (TA) muscle ($n = 311$ for WT-PBS (wild-type-phosphate-buffered saline) and $n = 1181$ for mKO(muscle-specific knockout)-PBS, $^*P < 0{,}001$) and significantly reduced 4 weeks after viral injection ($n = 487$ for mKO-AAV, $^*P < 0{,}001$). (**B**) Histological aspect of myotubularin-deficient skeletal muscle 4 weeks after rAAV2/1-CMV-Mtm1 transfer. Hematoxylin and eosin, HE (upper panels, magnification $\times 400$) and nicotimanide adenine dinucleotide tetrazolium reductase (NADH-TR) (lower panels, $\times 630$) stainings of TA cross-sections from WT (left), mutant (middle) and AAV-treated (right) mice. Note the recovery of oxidative reactivity pattern in myotubularin-expressing mKO muscle. (**C**) Immunostaining of mKO muscle cross-sections 4 weeks after rAAV-Mtm1 injection with myotubularin antibodies (left) and Hoechst (middle). Right panel is the merge of MTM1 labeling and Hoechst. Right panel shows an inflammatory infiltrate in a region where myotubularin is highly overexpressed ($\times 400$).

structure where the excitation–contraction coupling takes place (Fig. 5C). Because of the size of the epitope–antibody–gold particle complex, it is not possible to distinguish between a location at the junctional sarcoplasmic reticulum and at the T-tubule within the triad. Overexpressed myotubularin, like the endogenous one, is present as a doublet in skeletal muscle by western blot (Fig. 5D), indicating that these isoforms result from post-translational modification of the protein rather than alternative splicing of the *Mtm1* gene. We also compared the distribution of endogenous and overexpressed myotubularin in skeletal muscle by subcellular fractionation. We found that, in both conditions, myotubularin is distributed in the cytosolic S3 fraction, containing glyceraldehyde-3-phosphate dehydrogenase (GAPDH), and in the membrane P3 fraction, containing caveolin 3 (which is associated with sarcolemmal caveolae) (Fig. 5D). These results suggest that overexpressed myotubularin has a similar distribution than the endogenous protein within muscle fibers and validate the use of AAV-mediated overexpression for functional studies.

Overexpressed myotubularin induces a plasma membrane pathology in skeletal muscle

In order to get insights into myotubularin function in skeletal muscle, we analyzed the effect of its overexpression. We

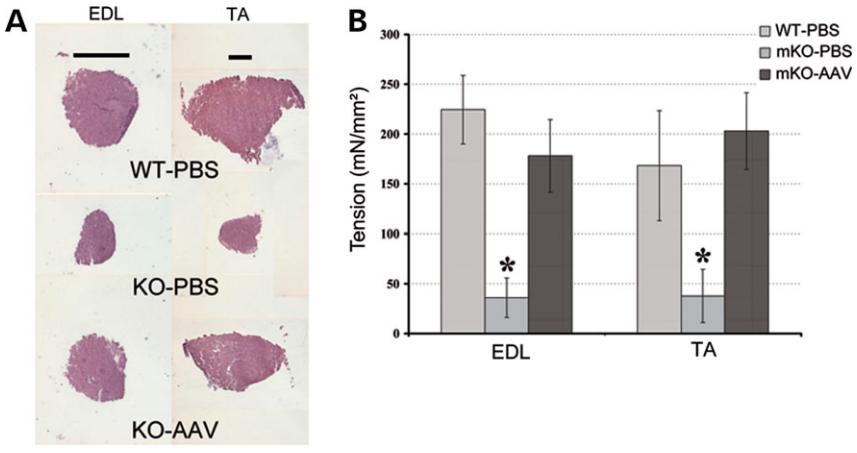

Figure 4. Recovery of the contractile force in *Mtm1*-deficient skeletal muscle. (**A**) Extensor digitorum longus (EDL) and tibialis anterior (TA) muscle cross-sections 4 weeks after viral injection. The photographs illustrate the important increase in the volume of both mutant muscles. The bars represent 1 mm. (**B**) The histogram represents the isometric contractile force (mean ± SD) of isolated EDL and TA normalized by muscle length. Strength was also measured 4 weeks after injection. Results show a significant decrease in muscle force between wild-type and mKO animals at 8 weeks of age ($^{*}P < 0.001$), whereas an important recovery of strength is observed after myotubularin treatment (force is about five times higher in treated versus untreated muscles, *P*-value between mKO-PBS (muscle-specific knockout-phosphate-buffered saline) and mKO-AAV (muscle-specific knockout-adeno-associated virus) is $P = 0.0006$ for both muscles).

injected a higher dose of rAAV2/1-CMV-Mtm1 vector (12×10^{10} vg) into the TA of 4 week-old WT animals. Mice were euthanized for analysis 6–8 weeks later (compared with 4 weeks in the former experiments). In these conditions, we observed a higher frequency of pathologic features in transduced fibers than with the gene therapy protocol. These pathological effects are specific for myotubularin overexpression as they were not observed when other rAAV2/1 vectors, containing either murine secreted alkaline phosphatase or green-fluorescence protein cDNAs under the same CMV (cytomegalovirus) promoter, were injected into skeletal muscle (data not shown). Figure 6A shows that myotubularin overexpression leads to the presence of vacuoles and needle-like structures in myofibers, as observed in semithin sections. Vacuoles were found in ~35% of muscle fibers and were caveolin-3, dystrophin and dihydropyridine receptor (DHPR)-positive but laminin 2-negative, indicating that they originate from the sarcolemma and/or T-tubules (Supplementary Material, Fig. S2). One can note that a few large vacuoles that are observed during the evolution of pathology in the *Mtm1* KO mouse (12) are similarly labeled by these membrane markers (Supplementary Material, Fig. S3). In AAV-transduced fibers, the large vacuoles are either empty or contain internal membranes (Fig. 6A and discussed later), suggesting in the latter case that they originate from the degeneration of the needle-like structures. Ultrastructural analysis of TA muscle overexpressing myotubularin revealed that the needle-like structures are highly organized membrane assemblies, which were often located in the subsarcolemmal region of the fiber (Fig. 6B). These were sometimes associated with honeycomb structures, typical of abnormal proliferation of the T-tubule system (26). Small autophagic vacuoles containing undigested material were also occasionally observed (Fig. 6B). We found by immunofluorescence and immunoelectron microscopy that myotubularin strikingly accumulates on these membrane assemblies and may thus contribute to their formation (Fig. 6C and Supplementary Material, Fig. S4). To better understand the organization of these myotubularin-associated membranes, we performed electron-tomography experiments to reconstitute the three-dimensional (3D) architecture of these assemblies. Figure 6D shows that they are not tubules, as initially suggested by the electron microscopy features, but instead are formed by membrane saccules, often piled-up in an almost parallel, slightly twisted, arrangement. Upon interaction, the saccules form an electron dense interface with a constant width of 14–16 nm whereas the outermost saccule is closed by a thinner membrane ~7 nm wide. These measurements indicate that the electron dense interface is composed of two lipid bilayers held together at a constant distance probably through an interaction with an abundant adhesion molecule. Although they were often in close contact with the sarcolemma, we could not detect a direct continuity between the membrane of these saccules and the plasma membrane or other membranous compartments. However, we noticed the presence of vesicles that appear derived from the plasma membrane, which are loosely attached to the membranous proliferations (Fig. 6D). The morphological abnormalities found upon myotubularin overexpression had no detectable effect on the contractile force of isolated muscles (data not shown).

DISCUSSION

X-linked myotubular myopathy is, in most cases, a very severe and life threatening congenital disease that has no specific or curative treatment. In the present study, we have injected a recombinant rAAV2/1 vector expressing the *Mtm1* cDNA into the skeletal muscle of symptomatic XLMTM mice to test the efficiency of this therapeutic approach. Several successful gene therapy studies using AAV vectors in mouse models of human muscular diseases have been reported to date and, more recently,

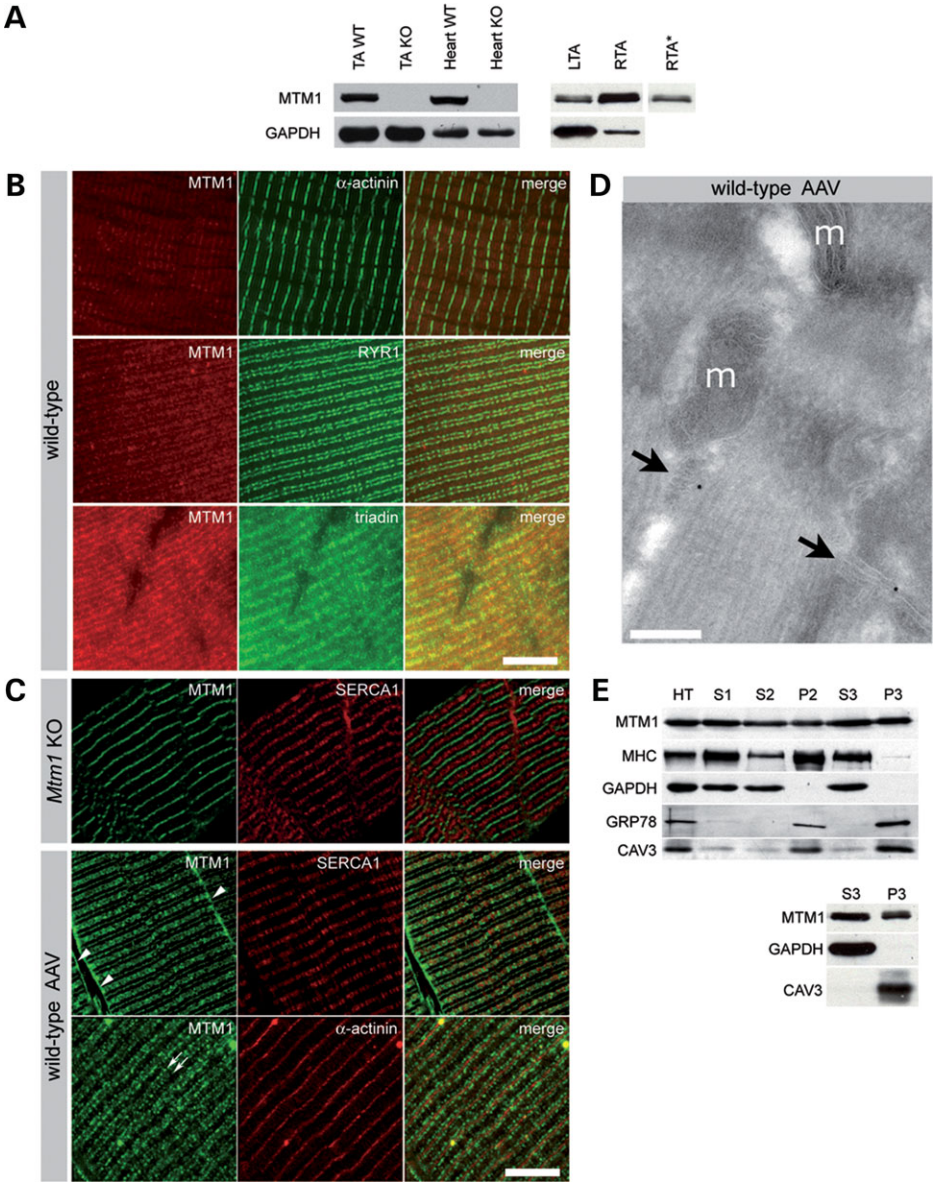

Figure 5. Subcellular localization of myotubularin in skeletal muscle**. (A)** Detection of endogenous myotubularin by western blot. Left panel shows the presence of myotubularin in wild-type (WT) but not KO skeletal muscle and heart. Glyceraldehyde-3-phosphate dehydrogenase (GAPDH) immunoreactivity was used as an internal control. Right panel illustrates the level of expression of myotubularin 6 weeks after adeno-associated virus (AAV) injection; 75 and 7.5 μg of proteins were loaded for phosphate-buffered saline (PBS) (LTA) and AAV (RTA)-injected WT muscles, respectively. A lower exposure of myotubularin band in RTA (RTA*) is shown to illustrate the doublet. (**B**) Localization of endogenous myotubularin in skeletal muscle. Semithin cryosections (0.5 μm) of WT muscle were stained for MTM1 (myotubularin), α-actinin (Z-lines), ryanodine receptor (RYR) and triadin (both in triads). Occasional α-actinin-positive Z-lines appear yellow when oblique orientation of the sarcomeres in sections superimpose the Z-lines with the adjacent triadic regions. The bar represents 5 μm. (**C**) Localization of overexpressed myotubularin in skeletal muscle. Semithin *Mtm1*-deficient (upper panels) and WT-AAV (middle and lower panels) muscle cryosections were stained for MTM1, SERCA1 (sarco-endoplasmic reticulum calcium ATPase 1) and α-actinin. Myotubularin antibody binds aspecifically to a region between I-bands in WT and KO myofibers, which probably corresponds to the M-band. Note myotubularin location at the sarcolemma (arrowheads) and around the Z-line (arrows) in WT-AAV muscle. The Z-line and I-band (endoplasmic reticulum) were labeled with antibodies against α-actinin and SERCA1, respectively. The bar represents 5 μm. (**D**) Subcellular localization of overexpressed myotubularin by immunoelectron microscopy. Triads (arrows) are labeled by r1947-coupled gold particles. Note the position of mitochondria (m, bar represents 200 nm). (**E**) Subcellular fractionation of skeletal muscle overexpressing myotubularin (upper panel) and wild-type muscle (lower). Proteins from total homogenate (HT), S1 (supernatant at 1000*g*), S2 (10 000*g*), S3 (100 000*g*) and the corresponding pellet fractions (P1, P2 and P3) were analyzed by immunoblotting. Myotubularin is distributed along all fractions. We used myosin heavy chain (MHC) and GAPDH as internal controls for cytosolic fractions. GRP78/BiP and caveolin 3 (CAV3) immunoreactivities are indicative of membrane fractions. Antibody r1947 was used in all illustrated experiments.

a protocol combining a brief course of immunosupression to rAAV delivery in a dog model of Duchenne muscular dystrophy has shown a sustained expression of the transgene product in muscles (27–31). We show that the XLMTM phenotype can be corrected in murine muscle by virally mediated *Mtm1* replacement. A vector expressing myotubularin under the CMV promoter was injected into the TA of muscle-specific mutant mice (mKO) at 4 weeks of age, when pathology and

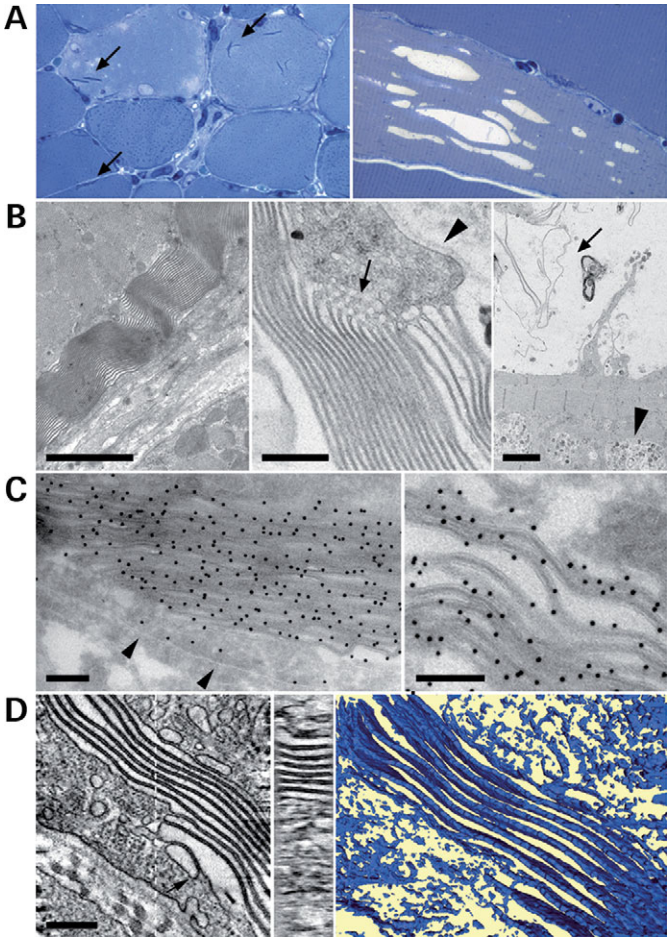

Figure 6. Effect of overexpression of myotubularin in skeletal muscle. (**A**) Presence of needle-like structures (left panel, arrows) and vacuoles (right panel) in wild-type muscle overexpressing myotubularin. Semithin cross-sections of tibialis anterior were stained with toluidine blue (×630, left and ×1000, right). (**B**) Electron micrographs illustrate the nature of myotubularin-induced needle-like structures (left and middle panels). They resemble myelin-like structures and are occasionally associated with honey combs-like structures (arrow, middle panel). Note that the basal lamina (arrowhead) is not included. Vacuoles often contain degenerative membrane aggregates (arrow, right panel). Occasional authophagic vacuoles are also present (arrowhead). Bars represent 2 μm in the left and right panels and 400 nm in the middle panel. (**C**) Immunogold detection with an anti-myotubularin antibody shows labeling of the sarcolemma (arrowheads) and an intense signal on the membrane aggregates. Bars indicate 200 nm. (**D**) Left panel: central section of an electron tomogram from a cellular region containing such a membrane assembly. Membrane sheets clearly appear as being composed of two bilayers. Vesicular structures can be found attached to the membrane sheets (arrow). Central panel: section through the membrane assembly normal to the section plane as indicated by the dotted line in the left panel. This cross-section demonstrates that the lipid assemblies are flat layers and not tubular structures. Right panel: surface representation of the lipid layers which evidences the twisted nature of the close to parallel lipid assemblies. The bar represents 200 nm in the left and central panels and 125 nm in the right panel.

muscle weakness were already present (mice were in clinical phase II, see 12). At this age, mKO myofibers are hypotrophic and contain mislocalized mitochondria, whereas most nuclei are still at their normal position beneath the sarcolemma. This suggests that, in mice, myotubularin might be primarily involved in myofiber growth and internal organelle positioning.

Four weeks after rAAV2/1-CMV-Mtm1 injection, XLMTM muscle histology was strikingly corrected, in particular, there was an overall increase in muscle and myofiber volume. Transduced mutant fibers showed a normal architecture with most nuclei at the periphery and an even distribution of mitochondrial NADH-TR staining, compared with the presence of internalized nuclei and mislocalized mitochondria in untreated muscle at this age. In 8 week-old mutant TA, many nuclei were detached from the sarcolemma and internalized but not necessarily at the centre of myofibers. Centralization of nuclei appears thus as a progressive event and varies between muscles, as previously described (12). Myotubularin replacement in mutant muscle also led to the recovery of contractile force deficits, which could even be visualized at the clinical level. This functional benefit was already observed 2 weeks post-injection (data not shown). Some signs of inflammation were observed in mKO muscle 4 weeks after rAAV2/1-CMV-Mtm1 injection that can be attributed to high expression of the transgene, without apparent repercussion on motor activity. The long-term effect of this vector could not be assessed as XLMTM mice die early during postnatal life (12). It will thus be important to test whether myotubularin replacement in most skeletal musculature by systemic delivery of rAAV vectors (32, 33) prolongs survival of *Mtm1* mutant mice. Recently, a spontaneous dog model of myotubular myopathy has been identified and may represent a useful model to further extend studies of gene therapy in the future if a colony can be established (Shelton G.D., www.wms2007.com/download/Full%20programme.pdf).

Apparently low levels of myotubularin expression in skeletal muscle had previously precluded determination of myotubularin's subcellular localization in this tissue. However, development of the new r1947 antibody, together with the use of AAV-mediated transduction to overexpress myotubularin, permitted us to demonstrate that it preferentially localizes to the triadic region, and perhaps also to the sarcolemma. Immunostaining of normal quadriceps semithin sections revealed a sarcomeric pattern of three bands; two specific ones flanking the Z-lines and co-localizing with ryanodine receptors and triadin, and a third non-specific band, seen in myotubularin-deficient muscle, at the M-line. Confocal microscopic examination of AAV transduced muscle overexpressing myotubularin revealed considerably stronger signal at the triads and specific localization at the sarcolemma as well. This sarcolemmal staining demonstrates that myotubularin is certainly capable of membrane association at this site; although it is presently unclear whether biologically significant amounts of endogenous protein are present there. Given this propensity to associate with the plasma membrane, we believe that triadic myotubularin may bind at T-tubules which are the plasma membrane invaginations that, together with terminal cisternae of sarcoplasmic reticulum, form the triads where excitation–contraction coupling occurs (34). Subcellular fractionation studies provided further confirmation that the localization of overexpressed myotubularin in muscle likely corresponds to that of the endogenous protein as they revealed a similar pattern of distribution. These results contrast with previous studies showing that endogenous myotubularin is mainly cytoplasmic in C2C12 myotubes (20) and suggest that it associates with sarcolemma and triads only upon myofiber maturation. The inability to

observe an abnormal morphological phenotype in cultures of well-differentiated myotubes from XLMTM patients suggests indeed that myotubularin plays a specific and non-redundant function in mature myofibers (35).

Our results indicate that when highly overexpressed in skeletal muscle, myotubularin alters membrane homeostasis leading to the formation of packed membrane assemblies close to the sarcolemma and of vacuoles that are positive for dystrophin, caveolin-3 and DHPRα, markers of plasma membrane and T-tubules. Electron tomography experiments showed that these structures are piled membrane structures, which form large and flat saccules. We propose that myotubularin-induced membrane assemblies originate either from the aggregation and fusion of endocytic vesicles or from plasma membrane remodeling. Several studies have shown that caveolin-3 containing caveolae, which are plasma membrane invaginations contribute to T-tubule biogenesis by the formation of reticular T-tubule elements in the absence of caveolae fission (36,37). Thus, it may be possible that excessive caveolae formation upon myotubularin overexpression contributes to the formation of these membrane structures. Abnormal oblique and longitudinal T-tubules have been observed in muscle biopsies from some XLMTM patients (38). Myotubularin could thus be implicated in remodeling longitudinal T-tubules to become transverse and in the maintenance of triads. Defects in the organization of these membrane structures would result in impairment of excitation–contraction coupling, leading to muscle weakness and atrophy (39). Recently, mutations in the amphyphisin 2/Bin1 gene in patients with an autosomal recessive form of CNM were shown to alter its membrane tubulation properties and interaction with dynamin 2 (6). Amphyphisin 2, which is located on T-tubules in muscle fibers, is involved in T-tubule biogenesis and appears essential for the organization of triads in Drosophila (40,41). Like in muscle biopsies from CNM patients, and in particular from patients carrying amphyphisin 2/Bin1 mutations (6,42), *Mtm1*-deficient murine muscle contains vacuoles positive for sarcolemma and T-tubule markers, such as caveolin 3 and DHPR-α. Similarly, biopsies from patients with hypokalaemic periodic paralysis, which is due to mutations in CaV1.1 (DHPR-α) or NaV1.4 (skeletal muscle voltage-gated sodium channel) leading to alterations in sarcolemmal depolarization, also contain similar vacuoles (42). Thus, these results suggest that defects in the excitation–contraction-coupling machinery may indeed be involved in XLMTM pathogenesis and that a functional link between myotubularin and amphyphisin 2 exists in skeletal muscle. An implication of membrane homeostasis and remodeling as an important pathomechanism in XLMTM and CNM is also supported by the striking involvement of other myotubularins (MTMR2 and MTMR13) and dynamin 2 in demyelinating neuropathies with abnormal myelin folding (13–15,43), and by the implication of the dynamin 2 gene in both autosomal dominant CNM and dominant intermediate Charcot-Marie-Tooth neuropathy type 2 (4,5,43,44).

Alternatively, albeit non-exclusively, the muscle pathology in XLMTM, and especially the striking muscle fiber hypotrophy might be related to the proposed involvement of myotubularin in the regulation of early and late endosomal function (23,24). The hypotrophy observed in *Mtm1*-deficient muscle fibers might result from defects in endocytosis of receptors involved in signaling pathways that are important for muscle growth, such as the insulin growth factor receptor 1, IGFR1 (45,46). The abnormal membrane structures observed upon AAV-mediated myotubularin overexpression in muscle could result from an imbalance between membrane internalization and recycling during endocytosis.

In conclusion, we provide evidence that myotubularin is partly a membrane-associated phosphatase in skeletal muscle fibers that plays an important role in plasma membrane homeostasis. In addition, our results indicate that gene therapy by local *Mtm1* transfer in skeletal muscle improves the strength of the targeted muscle in a mouse model of myotubular myopathy and might open novel strategies for treating this disorder.

MATERIALS AND METHODS

Generation of rAAV

Mouse *Mtm1* cDNA (AF073996, NCBI) was cloned by PCR with specific oligonucleotides containing restriction enzyme sites in the AAV expression plasmid pGG2-CMV-MCS plasmid in order to obtain the plasmid pGG2-Mtm1WT, where the *Mtm1* gene is under the transcriptional control of IE CMV promoter. Adenovirus-free pseudotyped AAV2/1 preparations were generated by tri-transfection of HEK293 cells with the plasmids pAAV2-CMV-Mtm1, pXX6 encoding adenovirus helper functions (47) and pLT-RCO2, which contains the AAV2 rep and AAV1 cap genes (a kind gift of R. Mulligan, Harvard University). Recombinants vectors were purified by double cesium chloride ultracentrifugation gradients from cell lysates, followed by dialysis against sterile PBS. Physical particles were quantified by real time PCR and vector titers are expressed as viral genomes per ml (vg/ml). The rAAV2/1-Mtm1 titer used in this study corresponds to 6.2×10^{12} viral genomes per ml (vg/ml).

Intramuscular delivery of AAV vectors

Four week-old male WT and Mtm1/HSA mice were anesthetized by intraperitoneal injection of 5 μl/body gram of ketamine (20 mg/ml, Virbac) and xylazine (0.4%, Rompun, Bayer). TA muscles were injected with 15 μl of either rAAV2/1-Mtm1 or sterile PBS solution. TA muscles were dissected under anesthesia 4–8 weeks after injection and frozen in nitrogen-cooled isopentane and liquid nitrogen for histological and immunoblot assays, respectively. Care and manipulation of mice were performed in accordance with national and European legislations on animal experimentation, and approved by the institutional ethical committee.

Antibodies

A C-terminal peptide (TSSSSQMVPHVQTHF) corresponding to amino acid residues 589–603 from mouse myotubularin was coupled with ovalbumin and injected into rabbits. Polyclonal antibodies were purified using the same peptide bound to Sulfolink Coupling Gel (Pierce) according to

manufacturer's instructions and dialyzed against PBS before storage. This antibody, r1947, was used for immunoblots and immunohistochemistry. Other antibodies used in this study are: monoclonal antibodies against glyceraldehyde-3-phosphate dehydrogenase (MAB374, Chemicon), caveolin 3 (610420, BD Transduction Laboratories), pan-myosin (MF20, Developmental Studies Hybridoma Bank) and rabbit polyclonal anti-GRP78 (PA1-014, Affinity BioReagents) for immunoblot analysis, and monoclonal anti-ryanodine receptor (clone 34C, Sigma), anti-triadin (clone IIG12, Sigma), anti-SERCA1 (sarco-endoplasmic reticulum calcium ATPase 1) (MA3-911, Affinity BioReagents) and anti-α-actinin (EA-53, Sigma) for immunohistochemistry.

Immunoblot analysis

Western blotting. Muscles were homogenized in 50 mM Tris, 10% glycerol, 1 mM EDTA, 50 mM KCl, 10 mM beta-glycerophosphate, 10 mM NaF, 1 mM Na_3VO_4, 0.1% SDS, 2% Triton X and protease inhibitors (PIC, Roche Diagnostics) using a Polytron homogenizer, kept in ice for 10 min, and centrifuged at 2000 rpm (5417R, Eppendorf) for 10 min. The supernatant was recovered and proteins were quantified with the Biorad Protein Assay detection kit. Proteins were transferred to nitrocellulose membranes.

Subcellular fractionation. TA muscles were homogenized in 10 mM $NaHCO_3$, 0.2 mM $CaCl_2$, PIC, and mixed in an equal volume of 500 mM sucrose, 300 mM KCl, 4 mM MgCl2, 60 mM histidine, pH 7.4. The suspension (total homogenate) was centrifuged at $1000 \times g$ for 20 min. The pellet (P1) was resuspended in PBS, 2% Triton X and PIC and the supernatant (S1) was further centrifuged at $10\,000 \times g$ for 20 min. The pellet (P2) was also resuspended in PBS, 2% Triton X and PIC, and the supernatant (S2) was centrifuged at 100 000*g* for 30 min. The supernatant (S3) was recovered as the cytosolic fraction and the pellet (P3) was washed in a solution containing 250 mM sucrose, 600 mM KCl, 3 mM MgCl2, 30 mM histidine, pH 7.4, and finally resuspended in PBS, 2% Triton X and PIC. Protein quantification was performed using the Biorad Protein Assay.

Immunohistochemistry and histological analysis

Immunohistochemistry. For immunofluorescence analysis of semithin muscle cryosections, animals were anesthetized and fixed by an intracardiac perfusion of 4% paraformaldehyde, 0.3% glutaraldehyde in PBS. The TA and quadriceps muscles were then dissected out and post-fixed in the same fixative for 2 h. After an overnight cryoprotection in 2.3 M sucrose in PBS containing 0.15 M glycine, biopsies were frozen in liquid nitrogen. Semithin cryosections of 500 nm were performed using a FCS cryo-chamber (Leica Microsystems) mounted on an Ultracut-S ultramicrotome (Leica Microsystems). Sections were incubated with blocking buffer (10% FCS in PBS) and stained overnight at 4°C with primary antibodies followed by washing and incubation with secondary antibodies (alexa 488 goat anti-rabbit IgG and alexa 594 goat anti-mouse IgG, Molecular Probes). For immunofluorescence on frozen-muscle, the TA was snap frozen in liquid nitrogen-cooled isopenthane and sections (7 μm) were obtained using a cryostat. Sections were first incubated with 5% bovine serum albumin (BSA) in PBS for 1 h at RT and then with r1947 (1:50 and 1:200, for semithin and frozen sections, respectively) in PBS-5% BSA-0.1% Brij35 (Sigma) at 37°C for 1 h 30 min. After several rinses in PBS-0.1% Brij35, secondary antibodies (goat anti-rabbit alexa 488 and goat anti-mouse-CY3, Molecular Probes) were incutated in PBS for 1 h. Samples were further rinsed and mounted with FluorSave reagent (Calbiochem) and analyzed with a confocal microscope (Leica).

Histology. Cross-sections (7 μm) of isopentane-frozen TA biopsies were stained with hematoxylin and eosin and analyzed using a Leica microscope coupled with a camera (Media Cybernetics). The area of muscle fibers and number of fibers with internal nuclei were measured using Metamorph software. For NADH-TR reaction, frozen sections were incubated with nitroblue tetrazolium (1 mg/ml, Sigma) and β-NADH (0 .4 mg/ml, Sigma) in 50 mM Tris–HCl, pH 7.3, at 57°C for 20 min.

Electron microscopy

Immuno-electron microscopy on thawed cryosections. Ultrathin cryosections of ∼70 nm were obtained at −110°C as described above. The immunogold was processed in an automat (EM IGL, Leica Microsystems) and consisted in: 15 min fixative quenching in 150 mM glycine, rinses in PBS, 30 min blocking in 0.1% BSA and 0.1% cold water fish skin gelatine (FSG, Aurion), 1 h incubation in primary antibody 1/100 in PBS containing 0.1% FSG, 1 h incubation with protein-A coupled with 10 nm colloidal gold particles (University Medical Center, Utrecht, NL) and postfixation in 2.5% glutaraldehyde.

Standard electron microscopy. Muscle biopsies from TA muscles of anesthetized mice were fixed with 2.5% glutaraldehyde in 0.1 M cacodylate buffer (pH 7.2) and processed as described (12). Semithin sections (2 μm) were stained with toluidine blue and ultrathin sections (70 nm) were observed using a Morgagni transmission electron microscope (FEI).

Electron tomography

For electron tomography, semithin sections (200–250 nm) were cut using an ultracut UC6 (Leica Microsystem), collected on formvar-carbon coated copper hexagonal 50 mesh grids and post-stained with 2% Uranyl acetate (W/V) and lead citrate. Ten nanometer colloidal gold particles were applied on one side of the grid to be used as fiducial markers. Automated data acquisition of the single tilt series through an angular range of −65° to +65° with 1° increments was performed using an electron microscope equipped with a field emission gun and operating at 200 kV (Tecnai F20, FEI Company, Eindhoven, The Netherlands) and Xplore 3D. Tomograms were computed using the SIRT algorithm within the Inspect3D tomography reconstruction package (FEI). Three-dimensional surface models were calculated with AMIRA.

Functional analysis

The isometric contractile properties of EDL and TA muscles were studied *in vitro*. Measurements were performed according to methods previously detailed (48). Muscles were dissected free from adjacent connective tissue and soaked in an oxygenated Krebs solution (95% O_2 and 5% CO_2) containing (mM): NaCl 118, $NaHCO_3$ 25, KCl 5, KH_2PO_4 1, $CaCl_2$ 2.5, $MgSO_4$ 1, glucose 5, maintained at a temperature of 20°C. Muscles were connected at one end to an electromagnetic puller and at the other end to a force transducer. After equilibration (45 min), stimulation (frequency of 125 Hz, train of stimulation of 300 ms) was delivered through electrodes running parallel to the muscle. Tetanus isometric contractions were recorded at L_0 (which is determined as the length at which maximal tetanus isometric force is observed). Maximal isometric titanic force (P_0) was measured. Specific P_0 (sP_0) was calculated by dividing the force by the estimated cross-section area (CSA) of the muscle. Assuming muscles have a cylindrical shape and a density of 1.06 mg mm^{-3}, CSA corresponds to the wet weight of the muscle divided by its fiber length (L_f).

SUPPLEMENTARY MATERIAL

Supplementary Material is available at HMG Online.

ACKNOWLEDGEMENTS

We wish to thank Nicolas Guerchet, Josiane Hergueux, Bernard Gjata and Natasha Darras for help in functional and histological studies. We are also grateful to Marie Liabeuf and members of IGBMC mouse house facility for help in animal care and Erwan Sourty (FEI) for help with the tomography software. We are grateful to Jocelyn Laporte for support and for critical reading of the manuscript. We also thank Arie Verklej (Utrecht University) for stimulating discussions.

Conflict of Interest statement. None declared.

FUNDING

This study was supported by funds from the Institut National de la Santé et de la Recherche Médicale, the Centre National de la Recherche Scientifique, the Hôpital Universitaire de Strasbourg (HUS), the Collège de France and by grants from the Association Française contre les Myopathies (AFM), the National Institutes of Health (P01 NS040828, K08 NS049095), the Muscular Dystrophy Association (USA), the Joshua Frase and Lee and Penny Anderson Family Foundations.

REFERENCES

1. Wallgren-Pettersson, C., Clarke, A., Samson, F., Fardeau, M., Dubowitz, V., Moser, H., Grimm, T., Barohn, R.J. and Barth, P.G. (1995) The myotubular myopathies: differential diagnosis of the X linked recessive, autosomal dominant, and autosomal recessive forms and present state of DNA studies. *J. Med. Genet.*, **32**, 673–679.
2. Laporte, J., Biancalana, V., Tanner, S.M., Kress, W., Schneider, V., Wallgren-Pettersson, C., Herger, F., Buj-Bello, A., Blondeau, F., Liechti-Gallati, S. *et al.* (2000) MTM1 mutations in X-linked myotubular myopathy. *Hum. Mutat.*, **15**, 393–409.
3. Laporte, J., Hu, L.J., Kretz, C., Mandel, J.L., Kioschis, P., Coy, J.F., Klauck, S.M., Poustka, A. and Dahl, N. (1996) A gene mutated in X-linked myotubular myopathy defines a new putative tyrosine phosphatase family conserved in yeast. *Nat. Genet.*, **13**, 175–182.
4. Bitoun, M., Maugenre, S., Jaeannet, P., Lacene, E., Ferrer, X., Laforet, P., Martin, J., Laporte, J., Lochmuller, H., Beggs, A. *et al.* (2005) Mutations in dynamin 2 cause dominant centronuclear myopathy. *Nat. Genet.*, **37**, 1207–1209.
5. Bitoun, M., Bevilacqua, J., Prudhon, B., Maugenre, S., Taratuto, A., Monges, S., Lubieniecki, F., Cances, C., Uro-Coste, E., Mayer, M. *et al.* (2007) Dynamin 2 mutations cause sporadic centronuclear myopathy with neonatal onset. *Ann. Neurol.*, **62**, 666–670.
6. Nicot, A., Toussaint, A., Tosch, V., Kretz, C., Wallgren-Pettersson, C., Iwarsson, E., Kingston, H., Garnier, J., Biancalana, V., Oldfors, A. *et al.* (2007) Mutations in amphiphysin 2 (BIN1) disrupt its membrane tubulation properties and its interaction with dynamin 2, and cause autosomal recessive centronuclear myopathy. *Nat. Gene.t*, **39**, 1134–1139.
7. Herman, G.E., Finegold, M., Zhao, W., de Gouyon, B. and Metzenberg, A. (1999) Medical complications in long-term survivors with X-linked myotubular myopathy. *J. Pediatr.*, **134**, 206–214.
8. McEntagart, M., Parsons, G., Buj-Bello, A., Biancalana, V., Fenton, I., Little, M., Krawczak, M., Thomas, N., Herman, G., Clarke, A. *et al.* (2002) Genotype-phenotype correlations in X-linked myotubular myopathy. *Neuromuscul. Disord.*, **12**, 939–946.
9. Mandel, J.-L., Laporte, J., Buj-Bello, A., Sewry, C. and Wallgren-Pettersson, C. (2002). In Karpati, G. (ed.), *Structural and Molecular basis of skeletal muscle diseases*. ISN Neuropath Press, Basel, pp. 124–129.
10. Pierson, C., Tomczak, K., Agrawal, P., Moghadaszadeh, B. and Beggs, A. (2005) X-linked myotubular and centronuclear myopathies. *J. Neuropathol. Exp. Neurol.*, **64**, 555–564.
11. Pierson, C., Agrawal, P., Blasko, J. and Beggs, A. (2007) Myofiber size correlates with MTM1 mutation type and outcome in X-linked myotubular myopathy. *Neuromuscul. Disord.*, **17**, 562–568.
12. Buj-Bello, A., Laugel, V., Messaddeq, N., Laporte, J., Pellissier, J.-F. and Mandel, L. (2002) The lipid phosphatase myotubularin is esential for skeletal muscle maintenance but not myogenesis in mice. *Proc. Natl Acad. Sci. USA*, **11**, 2297–2307.
13. Bolino, A., Muglia, M., Conforti, F.L., LeGuern, E., Salih, M.A., Georgiou, D.M., Christodoulou, K., Hausmanowa-Petrusewicz, I., Mandich, P., Schenone, A. *et al.* (2000) Charcot-Marie-Tooth type 4B is caused by mutations in the gene encoding myotubularin-related protein-2. *Nat. Genet.*, **25**, 17–19.
14. Azzedine, H., Bolino, A., Taieb, T., Birouk, N., Di Duca, M., Bouhouche, A., Benamou, S., Mrabet, A., Hammadouche, T., Chkili, T. *et al.* (2003) Mutations in MTMR13, a new pseudophosphatase homologue of MTMR2 and Sbf1, in two families with an autosomal recessive demyelinating form of Charcot-Marie-Tooth disease associated with early-glaucoma. *Am. J. Hum. Gene.t*, **72**, 1141–1153.
15. Senderek, J., Bergmann, C., Weber, S., Ketelsen, U., Schorle, H., Rudnik-Schoneborn, S., Buttner, R., Buchheim, E. and Zerres, K. (2003) Mutation of the SBF2 gene, encoding a novel member of the myotubularin family, in Charcot-Marie-Tooth neuropathy type 4B2/11p15. *Hum. Mol. Genet.*, **12**, 349–356.
16. Laporte, J., Bedez, F., Bolino, A. and Mandel, J. (2003) Myotubularins, a large disease-associated family of cooperating catalytically active and inactive phosphoinositides phosphatases. *Hum. Mol. Genet.*, **12 (Spec no. 2)**, R285–R292.
17. Robinson, F. and Dixon, J. (2006) Myotubularin phosphatases: policing 3-phosphoinositides. *Trends Cell Biol.*, **16**, 403–412.
18. Blondeau, F., Laporte, J., Bodin, S., Superti-Furga, G., Payrastre, B. and Mandel, J.L. (2000) Myotubularin, a phosphatase deficient in myotubular myopathy, acts on phosphatidylinositol 3-kinase and phosphatidylinositol 3-phosphate pathway. *Hum. Mol. Genet.*, **9**, 2223–2229.
19. Zhao, R., Qi, Y., Chen, J. and Zhao, Z.J. (2001) FYVE-DSP2, a FYVE domain-containing dual specificity protein phosphatase that dephosphorylates phosphatidylinositol 3-phosphate. *Exp. Cell Res.*, **265**, 329–338.

20. Laporte, J., Blondeau, F., Gansmuller, A., Lutz, Y., Vonesch, J.-L. and Mandel, L. (2002) The PtdIns3*P* phosphatase myotubularin is a cytoplasmic protein that also localizes to Rac1-inducible plasma membrane ruffles. *J. Cell Sci.*, **115**, 3105–3117.
21. Mochizuki, Y. and Majerus, P. (2003) Characterization of myotubularin-related protein 7 and its binding partner, myotubularin-related protein 9. *Proc. Natl Acad. Sci. USA*, **100**, 9768–9773.
22. Lorenzo, O., Unrbé, S. and Clague, M. (2005) Systematic analysis of myotubularins: heterodimeric interactions, subcellular localization and endosome-related functions. *J. Cell Sci.*, **119**, 2953–2959.
23. Cao, C., Laporte, J., Backer, J., Wandinger-Ness, A. and Stein, M. (2007) Myotubularin lipid phosphatase binds the hVPS15/hVPS34 lipid kinase complex on endosomes. *Traffic*, **8**, 1052–1067.
24. Tsujita, K., Itoh, T., Ijuin, T., Yamamoto, A., Shisheva, A., Laporte, J. and Takenawa, T. (2004) Myotubularin regulates the function of the late endosome through the GRAM domain-phosphatidylinositol 3,5-biphosphate interaction. *J. Biol. Chem.*, **279**, 13817–13824.
25. Wu, Z., Asokan, A. and Samulski, R. (2006) Adeno-associated virus serotypes: vector toolkit for human gene therapy. *Mol. Ther.*, **14**, 316–327.
26. Engel, A. and Banker, A. (2004) Ultrastructural changes in diseased muscle. In Engel, A. and Franzini-Armstrong, C. (eds), *Myology*. McGraw-Hill, pp. 762–766.
27. Goyenvalle, A., Vulin, A., Fougerousse, F., Leturcq, F., Kaplan, J., Garcia, L. and Danos, O. (2004) Rescue of dystrophic muscle through U7 snRNA-mediated exon skipping. *Science*, **306**, 1796–1799.
28. Blankinship, M., Gregorevic, P. and Chamberlain, J. (2006) Gene therapy strategies for Duchenne muscular dystrophy utilizing recombinant adeno-associated virus vectors. *Mol. Ther.*, **13**, 241–249.
29. Qiao, C., Li, J., Zhu, T., Draviam, R., Watkins, S., Ye, X., Chen, C., Li, J. and Xiao, X. (2005) Amelioration of laminin-alpha-2-deficient congenital muscular dystrophy by somatic gene transfer of miniagrin. *Proc. Natl Acad. Sci. USA*, **102**, 11999–12004.
30. Fougerousse, F., Bartoli, M., Poupiot, J., Arandel, L., Durand, M., Guerchet, N., Gicquel, E., Danos, O. and Richard, I. (2007) Phenotypic correction of a-sarcoglycan deficiency by intra-arterial injection of a muscle-specific serotype 1 rAAV vector. *Mol. Ther.*, **15**, 53–61.
31. Wang, Z., Kuhr, C., Allen, J., Blankinship, M., Gregorevic, P., Chamberlain, J., Tapscott, S. and Storb, R. (2007) Sustained AAV-mediated dystrophin expression in a canine model of Duchenne muscular dystrophy with a brief course of immunosuppression. *Mol. Ther.*, **15**, 1160–1166.
32. Wang, Z., Zhu, T., Qiao, C., Zhou, L., Wang, B., Zhang, J., Chen, C., Li, J. and Xiao, X. (2005) Adeno-associated virus serotype 8 efficiently delivers genes to muscle and heart. *Nat. Biotechnol.*, **23**, 321–328.
33. Denti, M., Rosa, A., D'Antona, G., Sthandier, O., De Angelis, F., Nicoletti, C., Allocca, M., Pansarasa, O., Parente, V., Musarò, A. *et al.* (2006) Body-wide gene therapy of Duchenne muscular dystrophy in the mdx mouse model. *Proc. Natl Acad. Sci. USA*, **103**, 3758–3763.
34. Karpati, G., Hilton-Jones, D. and Griggs, R. (2001)*Disorders of Voluntary Muscle.* Cambridge University Press.
35. Dorchies, O.M., Laporte, J., Wagner, S., Hindelang, C., Warter, J., Mandel, J. and Poindron, P. (2001) Normal innervation and differentiation of X-linked myotubular myopathy muscle cells in a nerve-muscle coculture system. *Neuromuscul. Disord.*, **11**, 736–746.
36. Parton, R., Way, M., Zorzi, N. and Stang, E. (1997) Caveolin-3 associates with developing T-tubules during muscle differentiation. *J. Cell Biol.*, **136**, 137–154.
37. Galbiati, F., Engelman, J., Volonte, D., Zhang, X., Minetti, C., Li, M., Hou, H.J., Kneitz, B., Edelmann, W. and Lisanti, M. (2001) Caveolin-3 null mice show a loss of caveolae, changes in the microdomain distribution of the dystrophin-glycoprotein complex, and t-tubule abnormalities. *J. Biol. Chem.*, **276**, 21425–21433.
38. Sarnat, H.B. (1990) Myotubular myopathy: arrest of morphogenesis of myofibers associated with persistence of fetal vimentin and desmin. Four cases compared with fetal and neonatal muscle. *Can. J. Neurol. Sci.*, **17**, 109–123.
39. Zhang, P., Chen, X. and Fan, M. (2007) Signaling mechanisms involved in disuse muscle atrophy. *Med. Hypotheses*, **69**, 310–321.
40. Razzaq, A., Robinson, I., McMahon, H., Skepper, J., Su, Y., Zelhof, A., Jackson, A., Gay, N. and O'Kane, C. (2001) Amphiphysin is necessary for organization of the excitation–contraction coupling machinery of muscles, but not for synaptic vesicle endocytosis in Drosophila. *Genes Dev.*, **15**, 2967–2979.
41. Lee, E., Marcucci, M., Daniell, L., Pypaert, M., Weisz, O., Ochoa, G., Farsad, K., Wenk, M. and De Camilli, P. (2002) Amphiphysin 2 (Bin1) and T-tubule biogenesis in muscle. *Science*, **297**, 1193–1196.
42. Inose, M., Higuchi, I., Nakagawa, M., Kashio, N. and Osame, M. (1999) Caveolin-3 and sarcoglycans in the vacuolar myopathies and centronuclear myopathy. *Muscle Nerve*, **22**, 1080–1086.
43. Zuchner, S., Noureddine, M., Kennerson, M., Verhoeven, K., Claeys, K., De Jonghe, P., Merory, J., Oliveira, S., Speer, M., Stenger, J. *et al.* (2005) Mutations in the pleckstrin homology domain of dynamin 2 cause dominant intermediate Charcot-Marie-Tooth disease. *Nat. Genet.*, **37**, 289–294.
44. Fabrizi, G., Ferrarini, M., Cavallaro, T., Cabrini, I., Cerini, R., Bertolasi, L. and Rizzuto, N. (2007) Two novel mutations in dynamin-2 cause axonal Charcot-Marie-Tooth disease. *Neurology*, **69**, 291–295.
45. Musaro, A., McCullagh, K., Paul, A., Houghton, L., Dobrowolny, G., Molinaro, M., Barton, E., Sweeney, H. and Rosenthal, N. (2001) Localized Igf-1 transgene expression sustains hypertrophy and regeneration in senescent skeletal muscle. *Nat. Genet.*, **27**, 195–200.
46. Chaussade, C., Pirola, L., Bonnafous, S., Blondeau, F., Brenz-Verca, S., Tronchère, H., Portis, F., Rusconi, S., Payrastre, B., Laporte, J. *et al.* (2003) Expression of myotubularin by an adenoviral vector demonstrates its function as a phosphatidylinositol 3-phosphate [PtdIns(3)P] phosphatase in muscle cell lines: involvement of PtdIns(3)P in insulin-stimulated glucose transport. *Mol. Endocrinol.*, **17**, 2448–2460.
47. Xiao, X., Li, J. and Samulski, R. (1998) Production of high-titer recombinant adeno-associated virus vectors in the absence of helper adenovirus. *J. Virol.*, **72**, 2224–2232.
48. Fougerousse, F., Gonin, P., Durand, M., Richard, I. and Raymackers, J. (2003) Force impairment in calpain 3-deficient mice is not correlated with mechanical disruption. *Muscle Nerve*, **27**, 616–623.